Received: 7 May 2022 | Revised: 3 June 2022 | Accepted: 6 June 2022

DOI: 10.1002/jemt.24184

PRIMERS IN MICROSCOPY

MICROSCOPY RESEARCH & TECHNIQUE WILEY

Measuring biological materials mechanics with atomic force microscopy - Determination of viscoelastic cell properties from stress relaxation experiments

Andreas Weber[1] | Rafael Benitez[2] | José L. Toca-Herrera[1]

[1]Institute of Biophysics, Department of Nanobiotechnology, University of Natural Resources and Life Sciences Vienna (BOKU), Vienna, Austria

[2]Departamento de Matemáticas para la Economía y la Empresa, Facultad de Economía, Universidad de Valencia, Valencia, Spain

Correspondence
Andreas Weber and José Luis Toca-Herrera, Institute of Biophysics, Department of Nanobiotechnology, University of Natural Resources and Life Sciences Vienna (BOKU), Muthgasse 11, Vienna, Austria.
Email: andreas.weber@boku.ac.at and jose.toca-herrera@boku.ac.at

Review Editor: Alberto Diaspro

Abstract

Cells are complex, viscoelastic bodies. Their mechanical properties are defined by the arrangement of semiflexible cytoskeletal fibers, their crosslinking, and the active remodeling of the cytoskeletal network. Atomic force microscopy (AFM) is an often-used technique for the study of cell mechanics, enabling time- and frequency-dependent measurements with nanometer resolution. Cells exhibit time-dependent deformation when stress is applied. In this work, we have investigated the stress relaxation of HeLa cells when subjected to a constant strain. We have varied the applied force (1, 2, 4, and 8 nN) and pause time (1, 10, and 60 s) to check for common assumptions for the use of models of linear viscoelasticity. Then, we have applied three models (standard linear solid, five element Maxwell, power law rheology) to study their suitability to fit the datasets. We show that the five element Maxwell model captures the stress relaxation response the best while still retaining a low number of free variables. This work serves as an introduction and guide when performing stress relaxation experiments on soft matter using AFM.

Research Highlights

- Cells exhibit linear viscoelastic properties when subjected to stress relaxation measurements at the studied different forces and times.
- The stress relaxation is best described by a five element Maxwell model.
- All three used models capture a softening and fluidization of cells when disrupting actin filaments.

KEYWORDS

atomic force microscopy, cell mechanics, linear viscoelasticity, relaxation time, viscosity

1 | INTRODUCTION

Biological materials such as cells are not isolated entities but exist in contact with other materials that exert mechanical stresses on them. In biology, many different examples of such stresses occur. Cells perform active deformations for migration purposes, shear stresses are exerted by fluid flows in the cardiovascular system, or whole tissues expand and deform during development and movement (Hallou & Brunet, 2020; Iskratsch et al., 2014; Jansen et al., 2015). The mechanics of the surrounding tissue, the mechanical interaction

of cells with each other and the active regulation of cell mechanical properties are integral factors to consider in cellular biology (Moeendarbary & Harris, 2014). Cells can feel and respond to the mechanical properties of their environment. This is important for stem cell differentiation, cell migration and in cases of disease (Engler et al., 2006; Hoffman & Crocker, 2009; Paluch et al., 2015). As an example, solid tumors are known to be stiffer than normal tissue due to extracellular matrix rearrangements, while cancer cells have been shown to behave softer both in vitro and in vivo (Plodinec et al., 2012; Zemła et al., 2017).

Eukaryotic cells are complex, hierarchical materials, and the different semi-flexible polymers that make up their cytoskeleton determine cell shape and mechanics (Fletcher & Mullins, 2010). The cytoskeleton gives the cells the ability to resist, adapt, and react to mechanical forces from the out- and the inside. The actin cytoskeleton and the actomyosin cortex are the main determinants of cell mechanical properties (Salbreux et al., 2012). In addition, other cytoskeletal polymers such as microtubules and intermediary filaments have been shown to be incremental for cell mechanics and shape changes (Herrmann et al., 2007; Rotsch & Radmacher, 2000; Weber, Iturri, Benitez, Zemljic-Jokhadar, & Toca-Herrera, 2019). Further, both the nucleus and the cytoplasm play roles in shaping cell mechanics.

Most methods to investigate cell mechanics rely on sample deformation via the application of stress in direct contact (Wu et al., 2018). These include the use of optical and magnetic tweezers, magnetic twisting cytometry, micropipette aspiration, parallel plate rheometry, and atomic force microscopy (AFM). Noncontact methods include particle tracking microrheology, optical stretching and microfluidic deformability cytometry. Due to the inherent possibilities and limitations of each of these techniques, they probe different aspects of the mechanics of the cells. Atomic force microscopy is the most often used technique, as it enables measurements of both local and global cell mechanics, in combination with other microscopic techniques and chemical modifications. Different measurement set-ups and a wide range of applied frequencies are additional advantages (Binnig et al., 1986; Gavara, 2017; Krieg et al., 2019). Drawbacks include the low throughput of cells (dozens to hundreds per hour), complex implementation and the need to thoroughly design and implement experimentation.

Eukaryotic cells display time-dependent deformation when experiencing stress, which is called viscoelasticity. These properties arise from the molecular build-up of cells, where monomers of cytoskeletal elements are self-assembled to complex networks of semi-flexible polymers that are dynamically cross-linked at various stages. In addition, these three-dimensional networks are actively restructured. Application of stress on cells leads to application of stress to the cytoskeletal and cellular structures, which all possess distinct relaxation times. It is therefore important to not only consider the elastic, instantaneous response of cells to stress application, but rather investigate the relationship of stress to strain over time.

Historically, experimental investigations of viscoelastic properties have been performed using either time or frequency experiments. The former includes the decay of stress at a given deformation (stress relaxation) and the increase of deformation at a given stress (creep experiment). The latter includes application of stresses toward the samples at different frequencies. In AFM measurements, the position of the cantilever is tightly controlled by a feedback circuit that enables performing both stress relaxation and creep experiments with control on the nanometer, piconewton, and millisecond scale. In recent years, cellular stress relaxation experiments by AFM have been used to investigate the viscoelastic properties of cells (Darling et al., 2007; Efremov et al., 2019; Hiratsuka et al., 2009; Moreno-Flores et al., 2010a; Okajima et al., 2007). Different studies have reported that cancer cells show a softer mechanical phenotype in comparison to healthy ones and that actin filaments are the major determinant of cell mechanical properties (Efremov et al., 2014; Lekka et al., 1999; Tavares et al., 2017).

A thorough investigation of the influence of the experimental set-up on the derived mechanical parameters is needed. For viscoelasticity measurements of cells by AFM this includes the shape of the indenter, applied forces, loading rate, time and more (Nawaz et al., 2012; Weber et al., 2021; Weber, Iturri, Benitez, & Toca-Herrera, 2019). The most often used models for data evaluation rely on assumptions of linear viscoelasticity. This means that the stress applied to the material is proportional to the strain at any given time and that the sum of strain outputs results from each stress inputs (Boltzmann superposition principle). These assumptions only hold up for a given material at a certain set of stresses, strains, experimental times, and temperatures. Applying a constant stress on a material (creep experiment) leads to an increase in deformation over time that is described by the creep compliance function $J(t)$. The decay of stress while keeping the strain constant (stress relaxation experiment) is described by the relaxation modulus function $E(t)$. For solving the integral functions analytically, combinations of springs (elastic elements) and dashpots (viscous dampers) are used to model the stress–strain response over time (Lim et al., 2006). Additional mechanical elements called springpots that are based on fractional calculus have been introduced (Bonfanti et al., 2020; Mainardi & Spada, 2011).

Recently, we have reported on the importance of loading rate, load (applied force) and indenter geometry when investigating the mechanical properties of cells using AFM (Weber et al., 2021; Weber, Iturri, Benitez, & Toca-Herrera, 2019). In this work, we focus on stress relaxation experiments performed on cells using spherical indenters at different loads (from 1 to 8 nN) and experimental times (1, 10, and 60 s). We then derive and apply three different models (standard linear solid, five element Maxwell model, power law model) to solve the relaxation modulus function and calculate the viscoelastic properties of the cells. In addition, we introduce the dimensionless Deborah number as intuitive parameter for understanding the viscoelastic properties of soft matter. Further, we check the applicability of the used models for measurements performed on cells with depolymerized actin filaments. This work should serve as an introduction and guide when performing stress relaxation experiments on soft matter using AFM.

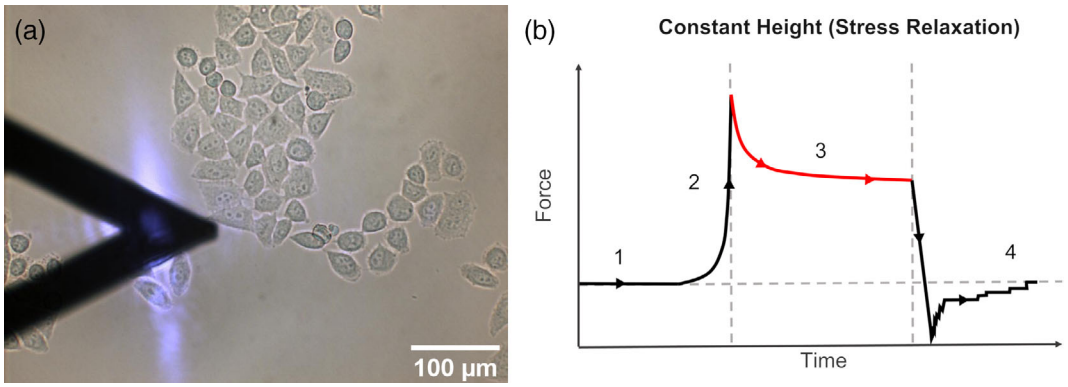

FIGURE 1 (a) Experimental set-up with cantilever, laser spot, and cell sample. The nuclei are visible in the micrograph and the piezo position was used to guide the measurement after optical calibration. (b) Representation of the force–time curve. Note that in 1 the AFM-tip approaches the cell, in 2 the tip is in contact with the cell, in 3 the cell reacts to the external stress (force relaxation), and in 4 the cantilever is retracted and the AFM-tip leaves the cell.

2 | MATERIALS AND METHODS

2.1 | Cell culture and sample preparation

HeLa cells (cervix carcinoma, purchased from ATCC) were grown in minimum essential medium (MEM) supplemented with 10% FBS (fetal bovine serum) and 1% penicillin/streptomycin. Cells were cultivated at 37°C with 5% CO_2 and 95% relative humidity at a maximum confluence of 80% and passaged twice per week. Before measurements, cells were trypsinized using TrypLE™ Express, centrifuged, resuspended in medium, and counted. For AFM measurements, borosilicate glass cover slips (diameter of 24 mm, thickness of around 0.1 mm) were rinsed with EtOH, N_2 dried and cleaned with oxygen plasma for 20 s. Then, 2×10^5 cells were added and incubated for 48 h. Prior to measurements, the samples were washed thrice with PBS and the medium was changed to Leibovitz L-15 medium. For actin disruption, cells were incubated for 30 min in 5 µM Cytochalasin D (see Figure S1, Supporting Information). All cell culture components were purchased from Thermo Fisher Scientific (Waltham, USA).

2.2 | Cantilever preparation

Triangular, tipless cantilevers NP-O B (Bruker, Germany) with a nominal stiffness of 0.12 N/m were cleaned with acetone, dried with nitrogen, and then further cleaned with UV/O treatment for 30 min. Then, a UV-curable glue (NOA68, Norland Optical Adhesives) was used to glue silica particles with a nominal diameter of 10 µm to the end of the cantilever. First, the end of the cantilever was tipped into the glue, and then a singled-out particle in water suspension was approached and contacted for 10 s at a force of 10 nN with the residual glue on the cantilever. The correct positioning of the particle at the central end of the cantilever was performed using the *x*- and *y*-motion of the piezo. Then, the cantilever was retracted 200 µm and the glue was first cured in liquid at 20°C for 30 min at a wavelength of 280 nm, followed by 30 min curing with UV-light in air and a final overnight curing step at 50°C. Cantilevers were visually inspected with light microscopy and cleaned as above before use. Cantilevers were calibrated using the thermal tune method (Butt & Jaschke, 1995).

TABLE 1 Indentation, contact area (assuming a parabolic contact profile), and stress for the applied forces of 1, 2, 4, and 8 nN.

Force (nN)	δ (µm)	A (µm^2)	σ (Pa)
1	1.00 ± 0.05	31.5 ± 1.4	31 ± 1
2	1.38 ± 0.04	43.4 ± 1.4	46 ± 2
4	2.06 ± 0.07	64.8 ± 2.3	62 ± 2
8	2.63 ± 0.07	82.7 ± 2.2	98 ± 3

2.3 | Atomic force microscopy measurements

Measurements were performed on a JPK Nanowizard III (Bruker, Germany), with a CellHesion module mounted on an inverted optical microscope (Axio Observer Z1, Zeiss) at 37°C in L-15 medium. Figure 1a shows the measurement set-up. An optical calibration was performed to overlay the microscopy image with *x*–*y*-positions of the AFM piezo. Stress relaxation experiments were performed on the nuclear regions of the cells, and at least 10 cells were measured per settings. Cells were approached with 5 µm/s and then the strain (deformation) was held constant at forces of 1, 2, 4, and 8 nN and for 1, 10, and 60 s. Then the cantilever was retracted at 5 µm/s. Curve lengths were set to 50 µm, and 1024 data points were sampled per second. Measurements were repeated thrice.

Figure 1b shows a representation of a typical experimental curve with the approach, pause, and retract segment. Table 1 shows the determined indentations and associated stresses for the different applied forces.

2.4 | Data analysis

The evaluation of the datasets was performed using the R afmToolkit, a free package for R developed by our group (Benítez et al., 2013; Benítez et al., 2017). Force curves were extracted with all segments using the JPKSPM software and imported into R. Then, contact and detachment points were determined using optimized parameters and

the force curves were corrected for their baseline. After this, the indentation was calculated. A single or double exponential function as well as a power law were fitted to the pause segment of the force-time curve (stress relaxation segment) using a Levenberg–Marquardt nonlinear least squares algorithm with optimized starting values. Further plotting and statistics were performed using OriginPro 2018 (OriginLab, USA).

2.5 | Stress relaxation analysis

The stress relaxation response $\sigma(t)$ (with $\sigma(t)=\frac{F(t)}{A(t)}$) of a linear viscoelastic body is defined as a hereditary integral by

$$\sigma(t)=\int_0^t G(t-\tau)\frac{d\varepsilon(\tau)}{d\tau}d\tau, \tag{1}$$

$G(t)$ is the relaxation shear modulus, t the time, ε the strain, and τ a time variable. For the case of stress relaxation AFM experiments, where the contact area does not decrease over time, the correspondence principle holds (Efremov et al., 2019; Findley et al., 1976), and the force relaxation reads as

$$F(t,\delta(t))=C_n\int_0^t G(t-\xi)\frac{\partial\delta^n(\xi)}{\partial\xi}d\xi. \tag{2}$$

Here $F(t,\delta(t))$ is the force, $\delta(t)$ is the indentation, C_n and n are constants depending on the shape of the indenter, and ξ is a dummy operator for integration. The Young's modulus E of a material is related to its Shear modulus via the Poisson ratio ν (set to 0.5) as

$$G=\frac{E}{2(1+\nu)}. \tag{3}$$

Usually, for instantaneous sample loading the Heaviside step function is used as an approximation to simplify the equations. The stress relaxation is then described by

$$F(t)=C_n\frac{E(t)}{(1-\nu^2)}\delta_0^n. \tag{4}$$

$E(t)$ is the relaxation Young's modulus and δ_0 is the constant deformation. This introduces an error to the evaluation that can be circumvented by applying the Lee–Radok approach to both the approach and the stress relaxation segment, which is omitted here (Lee & Radok, 1960). To solve the viscoelastic constitutive models, combinations of springs, dashpots and springpots are used. A spring behaves as ideally elastic ($\sigma(t)=k\varepsilon(t)$), while a dashpot behaves as ideal Newtonian fluid $\left(\sigma(t)=\eta\frac{d\varepsilon(t)}{dt}\right)$. A springpot is a fractional element to model a continuous relaxation spectrum and it is defined as

$$\sigma(t)=c_p\frac{d^\alpha\varepsilon(t)}{dt^\alpha} \tag{5}$$

here c_p is the so-called "firmness" of the material and α is a power law exponent. The exponent is 0 for linear elastic solids and 1 for viscous Newtonian liquids. Here, we have considered a standard linear solid in Maxwell representation (SLS), a 5-element Maxwell model (MW) and a single power law rheology model (PLR) were used (see Figure S2, Supporting Information).

For the SLS, the relaxation modulus is

$$E(t)=E_\infty+(E_1-E_\infty)e^{-t/\tau_1}, \tag{6}$$

while for the MW model, we obtain

$$E(t)=E_\infty+(E_1-E_\infty)e^{-t/\tau_1}+(E_2-E_\infty)e^{-t/\tau_2}. \tag{7}$$

E_∞ is the equilibrium modulus, E_1 and E_2 are the moduli of the respective Maxwell arms and τ_1 and τ_2 the relaxation times of the dampers. The viscosity of the dashpot is calculated as

$$\eta_i=E_i\tau_i. \tag{8}$$

For the SLS and MW models, the Deborah numbers De were calculated as

$$\mathrm{De}=\frac{\tau_i}{t_{\mathrm{Experiment}}}. \tag{9}$$

The Deborah number is a dimensionless rheological parameter used to estimate the fluidity of viscoelastic materials. When De is small the material behaves more fluid-like, while when De is large it behaves more solid-like.

The PLR model was used as

$$E(t)=\frac{E_\infty}{\Gamma(1-\beta)\Gamma(1+\beta)}\left(\frac{t}{t_0}\right)^{-\beta}. \tag{10}$$

Here Γ is the gamma function. Finally, a correction for the influence of the substrate on the measured mechanics was performed as

$$E_{\mathrm{corr}}=\frac{C_n}{1-\nu}E(t)\times(1+1.133\chi+1.283\chi^2+0.769\chi^3+0.0975\chi^4), \tag{11}$$

With

$$\chi=\frac{\sqrt{R\delta}}{h}, \tag{12}$$

with R as the radius of the indenter and h is the height of the sample (Dimitriadis et al., 2002).

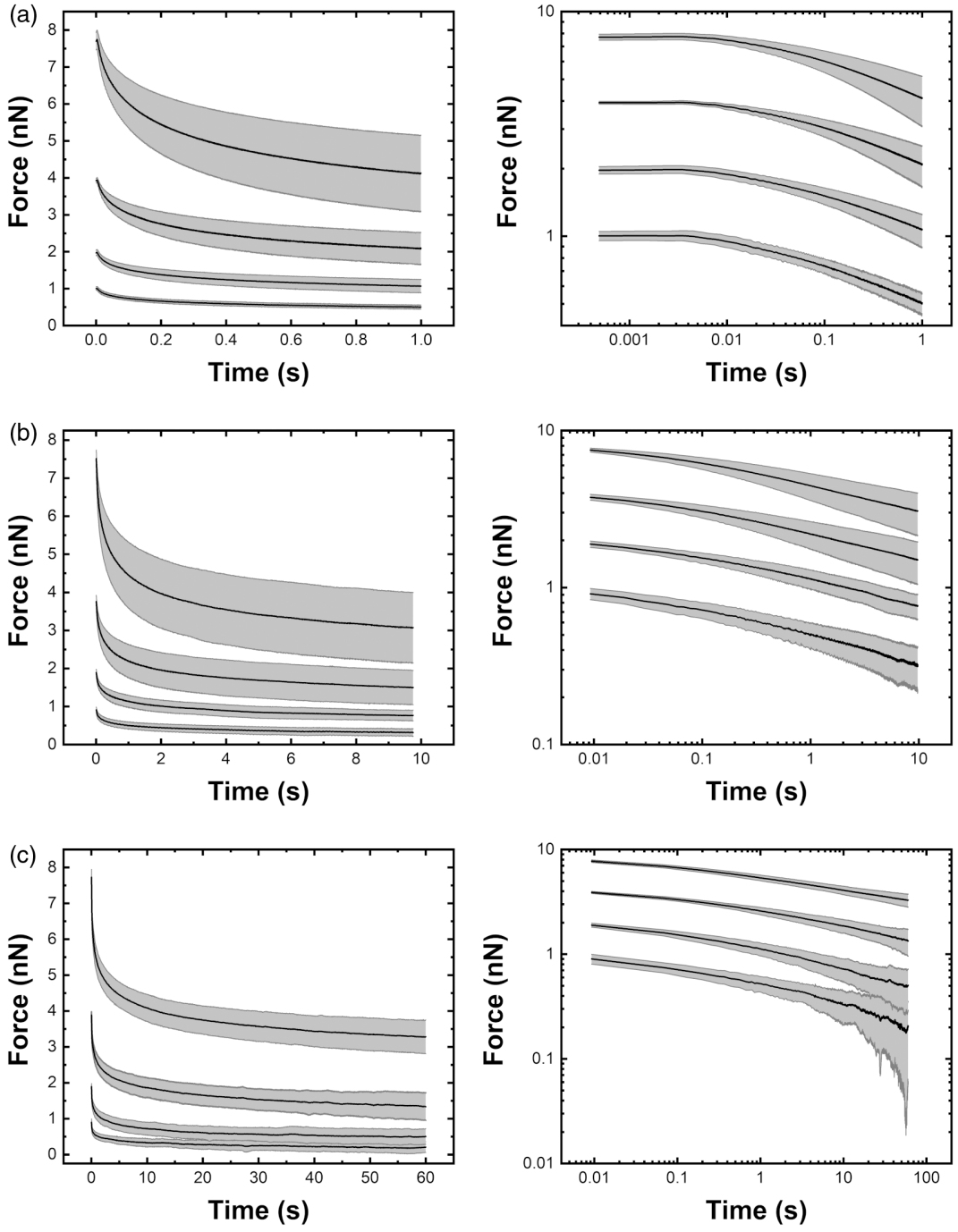

FIGURE 2 Averaged stress relaxation measurements (bold line averaged data, gray area standard error) for initial forces of 1, 2, 4, and 8 nN ((a) shows the data for 1 s, (b) for 10, and (c) for 60 s). The left column shows the force–time curves and the right column the logarithmic representation.

3 | RESULTS

3.1 | Averaging force–time curves for different loads and times

The stress relaxation experiments were pooled for the same experimental conditions (force and time) and averaged. Figure 2 shows the averaged curves with the associated standard error (all curves can be found in Figure S3, Supporting Information). For the 1 s curves, it is obvious that the stress relaxation process was not finished and that at least two distinct slopes are visible in the logarithmic plots. For both 10 and 60 s, the curve shapes are quite similar and asymptotic force values appear to be reached at around 3 for the 10 s measurements and at around 10 s for 60 s measurements. The initial force and the equilibrium force after relaxation depend on the maximum load at the beginning of the stress relaxation experiment. For the different force

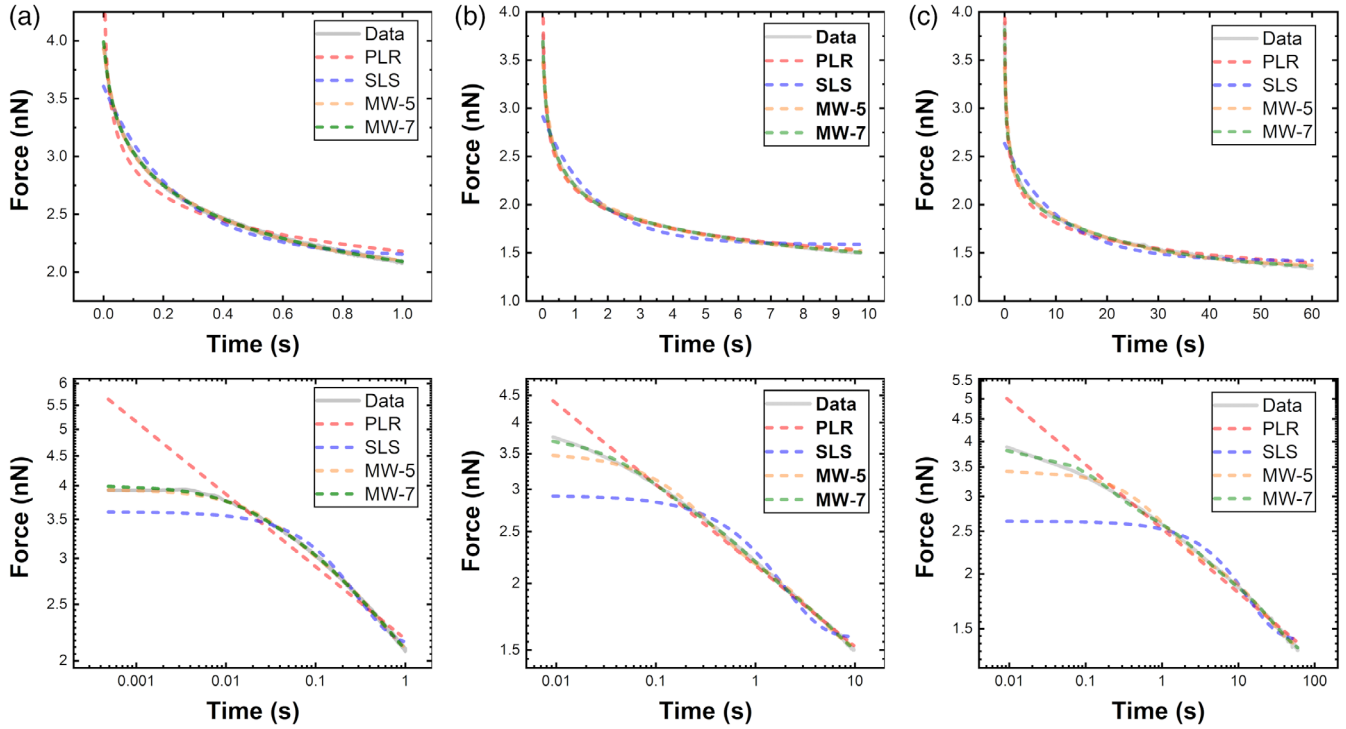

FIGURE 3 Fitting of the four chosen models (PLR—power law rheology (red), SLS—standard linear solid (blue), MW-5—5-element Maxwell model (orange), MW-7—7-element Maxwell model (green) for 1 s (a), 10 s (b), and 60 s (c) measurements.

set-points at defined experimental times, similar shapes of the curves are seen, therefore the assumptions of linear viscoelasticity appear to hold.

3.2 | Five-element Maxwell model is the best fitting model

The single force–time curves where then fitted with the SLS, MW, and PLR models. To qualitatively show the performance of the fitting procedures, the averaged curves were fitted (with an additional 7-element Maxwell model). Figure 3 shows these fittings for curves performed with an initial force of 4 nN for hold times of 1, 10, and 60 s (all fittings can be found in Figures S4–S7, Supporting Information). The analysis for all other experimental conditions can be found in the Supporting Information, Data S1. For the 1 s measurements, the PLR model performs the worst, followed by the SLS model. Both the five and the seven element MW model capture the shape of the curves very well. For longer experimental times, the PLR and the MW models perform reasonably well, while the SLS model does not. No significant difference in fitting performance can be seen between the MW-5 and the MW-7, indicating an over parameterization when using seven elements. Fitting analysis (R^2 and chi-square analysis) can be found in the supplemental information in Supporting Information, Table S1. For very short timescales in the millisecond range, the MW-7 model captures the relaxation process best. As this corresponds to only few data points, this must be taken with care.

3.3 | Mechanical properties do not scale with force or time

In the next step, the solutions for the PLR, SLS, and MW models were used to calculate the mechanical properties for the different experimental conditions. Figure 4 and Table 2 show the results for the PLR model (can be seen in Figure S8, Supporting Information). The power law exponent takes values from 0.15 to 0.4, which are in the range of what has already been published for different cell lines. For measurements with pause segments of 1 and 10 s, the exponent is similar, while for 60 s measurements it appears to be inversely correlated with the applied force. The modulus ranges from around 50 to 150 Pa and is comparable for all measurement conditions. A slight increase with the hold time can be seen for the modulus.

In addition to the PLR model, the SLS and MW model were also used to fit the data. Part of the results for the MW model can be seen in Figure 5 and Tables 3 and 4 (the whole results are found in the Figures S9–S11, Supporting Information). Interestingly, the equilibrium modulus appears to be scaling with the applied maximum force, while the moduli of the springs in both Maxwell arms stay constant for the used measurement parameters. In addition, two distinct Deborah numbers (derived from the relaxation times of the dashpots in the Maxwell arms) were identified. The one for the shorter relaxation time is influenced by measurement parameters at least for 1 and 10 s step holds, while the one for the longer relaxation time does not significantly differ. Calculated parameters for PLR and MW models can be found in Tables 2–4.

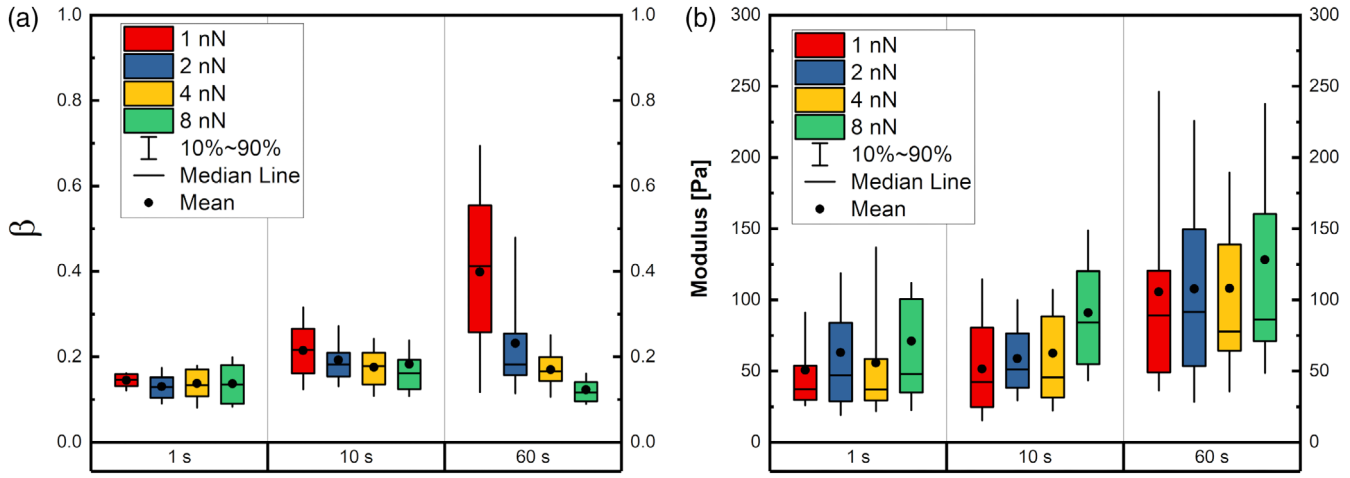

FIGURE 4 Power law rheological model. (a) Power law exponent for different forces (1, 2, 4, and 8 nN) and pause times (1, 10, and 60 s). (b) Corrected equilibrium modulus for the different measurement conditions.

TABLE 2 Parameters derived from power law rheological fittings (mean value ± SE of mean).

t (s)	*F* (nN)	E_∞ (Pa)	β
1	1	51 ± 8	0.14 ± 0.01
	2	63 ± 7	0.13 ± 0.01
	4	56 ± 11	0.14 ± 0.01
	8	71 ± 10	0.14 ± 0.01
10	1	51 ± 5	0.21 ± 0.01
	2	59 ± 4	0.19 ± 0.01
	4	63 ± 6	0.18 ± 0.01
	8	91 ± 7	0.18 ± 0.02
60	1	106 ± 15	0.40 ± 0.04
	2	108 ± 13	0.23 ± 0.02
	4	108 ± 15	0.17 ± 0.01
	8	128 ± 14	0.12 ± 0.01

3.4 | All models capture actin filament depolymerization

To test the ability of the models to capture differences in mechanical properties, cells were treated with Cytochalasin D (5 μM) for 30 min to disrupt actin filaments. Then, stress relaxation measurements with forces of 1, 2, 4, and 8 nN at pause times of 10 s were performed (see Figure S12–S15, Supporting Information). Actin filament disruption caused cells to become softer and more fluid like. Figure 6 shows the analysis performed with the PLR model (see Figure S16, Supporting Information). A significant decrease in the modulus can be seen. At the same time, the power law exponent increases significantly, indicating a fluidisation of the cells. Statistical analysis of these changes can be found in the Tables S2–S4, Supporting Information.

In a next step, the SLS and MW models were used. Figure 7 shows the moduli and Deborah numbers determined for the 5-element model (all data can be found in Figures S17–S19, Supporting Information). The equilibrium modulus and the modulus in the second Maxwell arm show a decrease, while the modulus in the first arm is similar for both conditions. The Deborah numbers of both Maxwell arms decrease, indicating a fluidization of the cells.

4 | DISCUSSION

In this work we discuss the usage of different models of linear viscoelasticity to model stress relaxation measurements performed on cells by AFM. To test the validity of the assumptions underlying linear viscoelasticity, measurements were performed using different forces (1, 2, 4, and 8 nN) and pause times (1, 10, and 60 s). Then, either combinations of springs and dashpots (SLS and MW) or just one single springpot (PLR) were used. This work aims to guide the reader and future performer of similar experiments on biological materials in how to properly plan, execute and model the data.

The variation of the applied force from 1 to 8 nN does not lead to significant changes in the calculated cell mechanical properties. The measured indentation follows the expected scaling with force as $F \propto \delta^{3/2}$. Therefore, the basic assumptions of linear viscoelasticity (proportionality of stress to strain) can be applied to the stress relaxation measurements.

A point to consider here is that the structure of cells is anisotropic, and therefore one could expect to measure different mechanical properties at changing indentation depth. In this study we have limited ourselves to the use of a spherical indenter with a radius of 5 μm. The pressure applied to the cell is distributed over the contact area which is in the range of dozens μm^2. The applied stress is distributed over a large volume of the cell and the resulting deformation is a superposition of deformation of all structures. Another case to consider is the use of nanometric, sharp tips: Here, the contact area is smaller and therefore the pressure on the deformed region is higher. As the tips are sharp (nanometer tip radius and low opening angle), individual regions with different

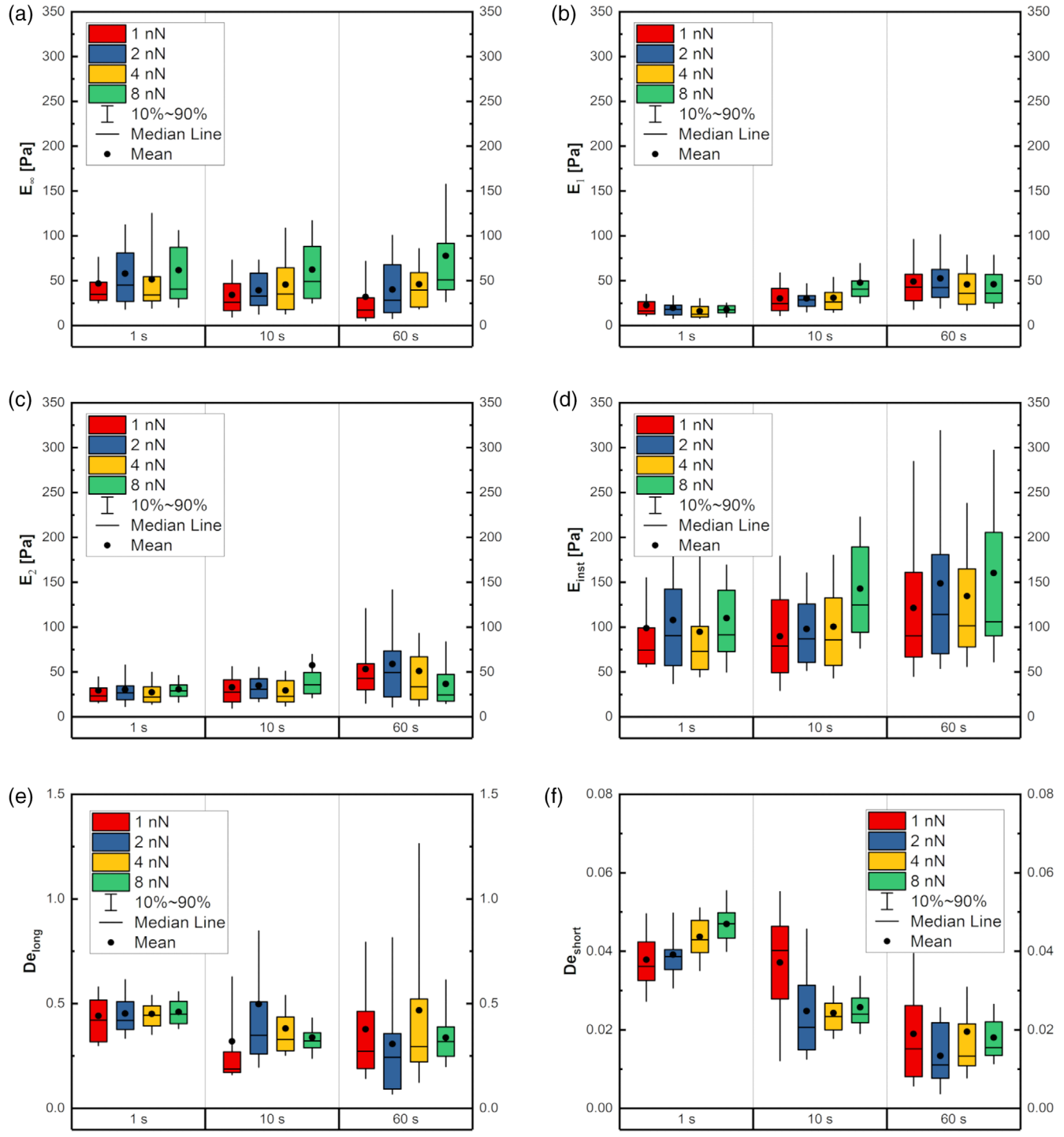

FIGURE 5 Five-element Maxwell model for stress relaxation measurements with 1, 2, 4, and 8 nN at pause times of 1, 10 and 60 s. (a) Equilibrium modulus, (b) modulus of spring in first Maxwell arm, (c) modulus of spring in second Maxwell arm, (d) instantaneous modulus, (e) Deborah number for long relaxation process, and (f) Deborah number for short relaxation process.

mechanics (such as single actin filaments or microtubules) can be identified (Garcia et al., 2020).

Combinations of springs and dashpots are widely used to describe the relation of stress to strain in the time domain. Here we have applied a standard linear solid and a 5-element Maxwell model. The SLS has one associated relaxation time, while the Maxwell model has two. Relaxation times of cells and cytoskeletal structures have been reported to be in the range of a few seconds (Efremov et al., 2021; Hiratsuka et al., 2009; Moreno-Flores et al., 2010b). Importantly, the measured relaxation times scale with the experimental time. It should therefore be considered with great care and the experimental time must be reported (Kollmannsberger & Fabry, 2011). The convenience

TABLE 3 Moduli and relaxation times derived from the five element Maxwell model fitting (mean value ± SE of mean).

t (s)	F (nN)	E_∞ (Pa)	E_1 (Pa)	E_2 (Pa)	E_{inst} (Pa)	τ_1 (s)	τ_2 (s)
1	1	47 ± 7	23 ± 4	29 ± 5	99 ± 16	0.04 ± 0.01	0.4 ± 0.1
	2	58 ± 6	20 ± 2	30 ± 3	108 ± 11	0.04 ± 0.01	0.5 ± 0.1
	4	51 ± 10	16 ± 2	27 ± 4	95 ± 16	0.04 ± 0.01	0.5 ± 0.1
	8	62 ± 7	18 ± 1	31 ± 2	110 ± 10	0.05 ± 0.01	0.5 ± 0.1
10	1	34 ± 4	30 ± 3	33 ± 4	90 ± 8	0.25 ± 0.02	3.2 ± 0.6
	2	39 ± 4	30 ± 2	35 ± 3	98 ± 7	0.24 ± 0.01	3.9 ± 2.0
	4	46 ± 7	31 ± 3	29 ± 3	101 ± 9	0.24 ± 0.01	3.8 ± 1.4
	8	62 ± 9	48 ± 6	58 ± 18	143 ± 9	0.26 ± 0.01	3.4 ± 1.2
60	1	32 ± 9	49 ± 6	53 ± 8	121 ± 17	1.14 ± 0.16	22.7 ± 4.0
	2	40 ± 7	53 ± 7	59 ± 8	149 ± 19	0.80 ± 0.09	19.1 ± 3.0
	4	46 ± 7	46 ± 6	51 ± 10	135 ± 17	1.17 ± 0.19	24.0 ± 3.9
	8	78 ± 9	46 ± 5	37 ± 4	160 ± 18	1.08 ± 0.07	20.3 ± 1.2

TABLE 4 Viscosities and Deborah numbers derived using the five element Maxwell model fitting (mean value ± SE of mean).

t (s)	F (nN)	η_1 (Pa s)	η_2 (Pa s)	De_{Short}	De_{long}
1	1	0.9 ± 0.1	13 ± 2	0.04 ± 0.01	0.44 ± 0.03
	2	0.8 ± 0.1	15 ± 3	0.04 ± 0.01	0.45 ± 0.02
	4	0.7 ± 0.1	13 ± 2	0.04 ± 0.01	0.45 ± 0.02
	8	0.8 ± 0.1	14 ± 1	0.05 ± 0.01	0.46 ± 0.01
10	1	6.5 ± 0.9	146 ± 22	0.04 ± 0.01	0.32 ± 0.06
	2	7.4 ± 0.9	168 ± 30	0.02 ± 0.01	0.49 ± 0.07
	4	7.6 ± 0.8	118 ± 15	0.02 ± 0.01	0.38 ± 0.02
	8	13.2 ± 2.8	148 ± 15	0.03 ± 0.01	0.34 ± 0.02
60	1	48.7 ± 7.7	986 ± 133	0.02 ± 0.01	0.38 ± 0.07
	2	42.9 ± 6.8	825 ± 167	0.01 ± 0.01	0.31 ± 0.05
	4	47.2 ± 8.2	961 ± 256	0.02 ± 0.01	0.47 ± 0.09
	8	48.6 ± 5.2	692 ± 73	0.02 ± 0.01	0.34 ± 0.02

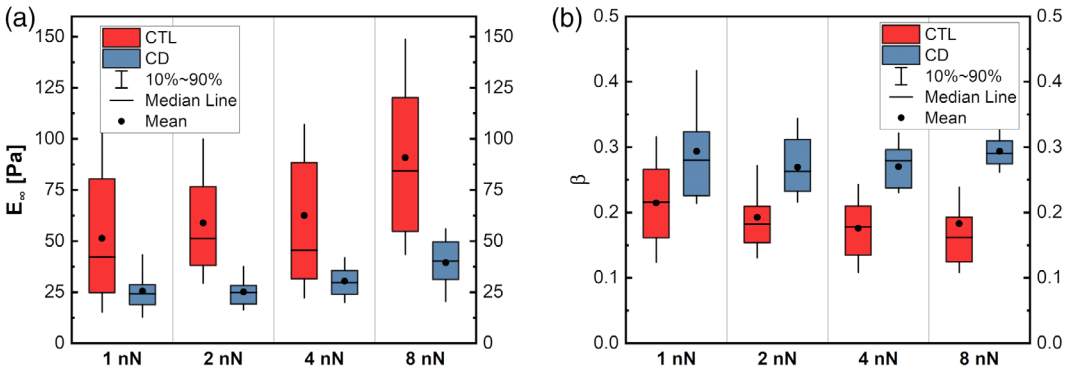

FIGURE 6 PLR model evaluation for control cells (red) and cytochalasin D treated cells (blue). (a) Equilibrium modulus. (b) Power law exponent.

of these models is the simply fitting procedure, and that the relaxation time scale describes a real physical relaxation process. One way to overcome the scaling is by normalizing the calculated relaxation times by the measurement times, thus resulting in the Deborah number. Our data indicates that the Deborah numbers for relaxation processes at shorter time-scales are inverse proportional to the experimental time. Multiple relaxation times (and addition of more Maxwell branches) have been used to assign relaxation processes to different cellular structures such as the membrane or the cytoskeleton. By removal of various cellular elements, one can test which individual

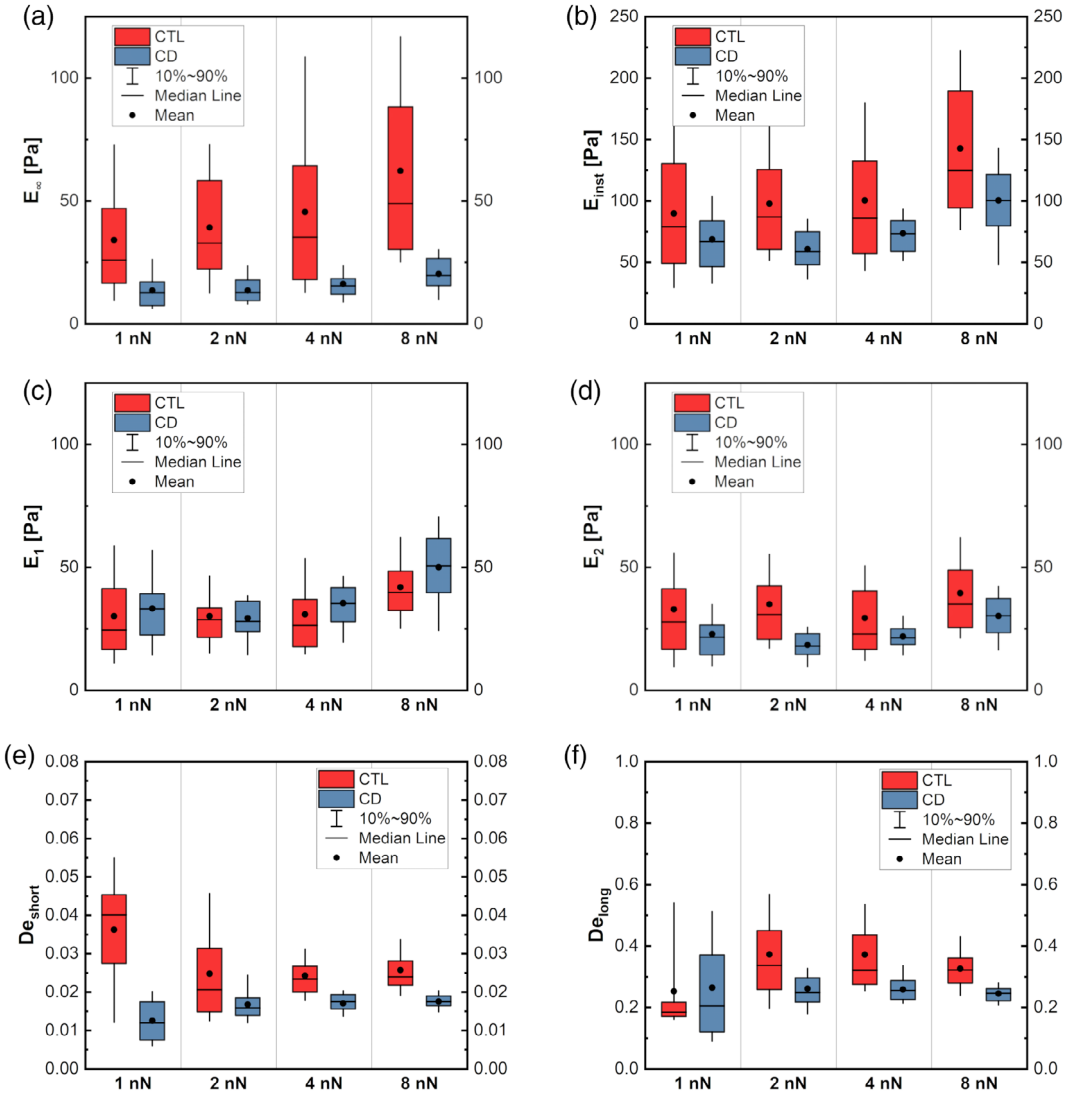

FIGURE 7 MW model evaluation for control cells (red) and cytochalasin D treated cells (blue). (a) Equilibrium modulus, (b) instantaneous modulus, (c) modulus of spring in first MW arm, (d) modulus of spring in second MW arm, (e) short Deborah number, and (f) long Deborah number.

mechanical elements are influenced. In the present work, we have depolymerized actin filaments using cytochalasin D. Both the PLR and SLS model show a softening and fluidization of the cells in all calculated parameters. Using the MW model shows that the stiffness of the first Maxwell branch does not decrease after actin filament removal, while the relaxation time decreases.

Cells are complex, hierarchical materials that undergo structural changes over time. As a result of that, they show a continuous relaxation spectrum. The application of linear viscoelastic models with distinct relaxation times only captures part of the relaxation process. To represent the relaxation spectrum, additional Maxwell branches can be added, and thus give rise to an arbitrary number of relaxation times. Increasing the number of fitting parameters comes with detriments: Computational time increases and the interpretation of physical meaning behind the relaxation times becomes more difficult. Recently, the continuous relaxation spectrum was described using fractional viscoelastic models. In the simplest case, a power law model (such as used here) can be defined by a springpot element. Such elements can then be integrated into classical linear viscoelastic models to in further detail investigate the relaxation processes of biological materials (de Sousa et al., 2020; Mainardi & Spada, 2011).

We show in the present work that for the applied forces and experimental time scales, all three used models can be applied to fit the datasets and calculate mechanical properties. Of those three models, the 5-element Maxwell model fits the data with the smallest error while providing possibility to investigate different relaxation time scales. The PLR performs well for fitting of curves with 10 and 60 s pause segments but does not capture the initial relaxation occurring at very short times. The SLS model does not fit any of the datasets well and should therefore only be used with care.

AUTHOR CONTRIBUTIONS

Andreas Weber, Rafael Benitez, José Luis Toca-Herrera: Conceptualization, methodology. **Andreas Weber:** experiments and formal analysis. **José Luis Toca-Herrera:** supervision. All authors contributed to writing, editing, and reviewing the manuscript.

ACKNOWLEDGMENTS

The authors want to thank Amsatou Andorfer-Sarr for supervision of the cell culture facilities.

FUNDING INFORMATION

This work was funded by the global budget of the Institute of Biophysics.

CONFLICT OF INTEREST

The authors declare no conflict of interest.

DATA AVAILABILITY STATEMENT

The data and measurements that support the findings of this study are available from the corresponding authors upon reasonable request.

ORCID

Andreas Weber https://orcid.org/0000-0001-6462-7687
Rafael Benitez https://orcid.org/0000-0002-9443-0209
José L. Toca-Herrera https://orcid.org/0000-0001-8951-2616

REFERENCES

Benítez, R., Bolós, V. J., & Toca-Herrera, J. L. (2017). afmToolkit: An R package for automated AFM force-distance curves analysis. *The R Journal*, *9*(December), 291–308. https://journal.r-project.org/archive/2017/RJ-2017-045/index.html

Benítez, R., Moreno-flores, S., Bolós, V. J., & Toca-Herrera, J. L. (2013). A new automatic contact point detection algorithm for AFM force curves. *Microscopy Research and Technique*, *76*(8), 870–876. https://doi.org/10.1002/jemt.22241

Binnig, G., Quate, C., & Gerber, C. (1986). Atomic Force Microscope. *Physical Review Letters.*, *56*, 930–933. https://doi.org/10.1103/PhysRevLett.56.930

Bonfanti, A., Kaplan, J. L., Charras, G., & Kabla, A. (2020). Fractional viscoelastic models for power-law materials. *Soft Matter*, *16*(26), 6002–6020. https://doi.org/10.1039/D0SM00354A

Butt, H.-J., & Jaschke, M. (1995). Calculation of thermal noise in atomic force microscopy. *Nanotechnology*, *6*(1), 1–7. https://doi.org/10.1088/0957-4484/6/1/001

Darling, E. M., Zauscher, S., Block, J. A., & Guilak, F. (2007). A thin-layer model for viscoelastic, stress-relaxation testing of cells using atomic force microscopy: Do cell properties reflect metastatic potential? *Biophysical Journal*, *92*(5), 1784–1791. https://doi.org/10.1529/biophysj.106.083097

de Sousa, J. S., Freire, R. S., Sousa, F. D., Radmacher, M., Silva, A. F. B., Ramos, M. V., Monteiro-Moreira, A. C. O., Mesquita, F. P., Moraes, M. E. A., Montenegro, R. C., & Oliveira, C. L. N. (2020). Double power-law viscoelastic relaxation of living cells encodes motility trends. *Scientific Reports*, *10*(1), 4749. https://doi.org/10.1038/s41598-020-61631-w

Dimitriadis, E. K., Horkay, F., Maresca, J., Kachar, B., & Chadwick, R. S. (2002). Determination of elastic moduli of thin layers of soft material using the atomic force microscope. *Biophysical Journal*, *82*(5), 2798–2810. https://doi.org/10.1016/S0006-3495(02)75620-8

Efremov, Y. M., Lomakina, M. E., Bagrov, D. V., Makhnovskiy, P. I., Alexandrova, A. Y., Kirpichnikov, M. P., & Shaitan, K. V. (2014). Mechanical properties of fibroblasts depend on level of cancer transformation. *Biochimica et Biophysica Acta - Molecular Cell Research*, *1843*(5), 1013–1019. https://doi.org/10.1016/j.bbamcr.2014.01.032

Efremov, Y. M., Kotova, S. L., Khlebnikova, T. M., & Timashev, P. S. (2021). A time-shift correction for extraction of viscoelastic parameters from ramp-hold AFM experiments. *Japanese Journal of Applied Physics*, *60*, SE1002. https://doi.org/10.35848/1347-4065/abf2d6

Efremov, Y. M., Okajima, T., & Raman, A. (2019). Measuring viscoelasticity of soft biological samples using atomic force microscopy. *Soft Matter*, *16*(1), 64–81. https://doi.org/10.1039/c9sm01020c

Engler, A. J., Sen, S., Sweeney, H. L., & Discher, D. E. (2006). Matrix elasticity directs stem cell lineage specification. *Cell*, *126*(4), 677–689. https://doi.org/10.1016/j.cell.2006.06.044

Findley, W. N., Lai, J. S., & Onaran, K. (1976). Chapter 5. Linear viscoelastic constitutive equations. In *Creep and relaxation of nonlinear viscoelastic materials*. Elsevier, Amsterdam. https://doi.org/10.1016/B978-0-7204-2369-3.50008-4

Fletcher, D. A., & Mullins, R. D. (2010). Cell mechanics and the cytoskeleton. *Nature*, *463*(7280), 485–492. https://doi.org/10.1038/nature08908

Garcia, P. D., Guerrero, C. R., & Garcia, R. (2020). Nanorheology of living cells measured by AFM-based force–distance curves. *Nanoscale*, *12*(16), 9133–9143. https://doi.org/10.1039/C9NR10316C

Gavara, N. (2017). A beginner's guide to atomic force microscopy probing for cell mechanics. *Microscopy Research and Technique*, *80*(1), 75–84. https://doi.org/10.1002/jemt.22776

Hallou, A., & Brunet, T. (2020). On growth and force: Mechanical forces in development. *Development*, *147*(4), dev187302. https://doi.org/10.1242/dev.187302

Herrmann, H., Bär, H., Kreplak, L., Strelkov, S. V., & Aebi, U. (2007). Intermediate filaments: From cell architecture to nanomechanics. *Nature Reviews Molecular Cell Biology*, *8*(7), 562–573. https://doi.org/10.1038/nrm2197

Hiratsuka, S., Mizutani, Y., Toda, A., Fukushima, N., Kawahara, K., Tokumoto, H., & Okajima, T. (2009). Power-law stress and creep relaxations of single cells measured by colloidal probe atomic force microscopy. *Japanese Journal of Applied Physics*, *48*, 08JB17 (4 pages) (8 PART 3). https://doi.org/10.1143/JJAP.48.08JB17

Hoffman, B. D., & Crocker, J. C. (2009). Cell mechanics: Dissecting the physical responses of cells to force. *Annual Review of Biomedical Engineering*, *11*, 259–288. https://doi.org/10.1146/annurev.bioeng.10.061807.160511

Iskratsch, T., Wolfenson, H., & Sheetz, M. P. (2014). Appreciating force and shape — The rise of mechanotransduction in cell biology. *Nature Reviews Molecular Cell Biology*, *15*(12), 825–833. https://doi.org/10.1038/nrm3903

Jansen, K. A., Donato, D. M., Balcioglu, H. E., Schmidt, T., Danen, E. H. J., & Koenderink, G. H. (2015). A guide to mechanobiology: Where biology and physics meet. *Biochimica et Biophysica Acta—Molecular Cell Research*, *1853*(11, Part B), 3043–3052. https://doi.org/10.1016/j.bbamcr.2015.05.007

Kollmannsberger, P., & Fabry, B. (2011). Linear and nonlinear rheology of living cells. *Annual Review of Materials Research*, *41*(1), 75–97. https://doi.org/10.1146/annurev-matsci-062910-100351

Krieg, M., Fläschner, G., Alsteens, D., Gaub, B. M., Roos, W. H., Wuite, G. J. L., Gaub, H. E., Gerber, C., Dufrêne, Y. F., & Müller, D. J. (2019). Atomic force microscopy-based mechanobiology. *Nature Reviews Physics*, *1*(1), 41–57. https://doi.org/10.1038/s42254-018-0001-7

Lee, E. H., & Radok, J. R. M. (1960). The contact problem for viscoelastic bodies. *Journal of Applied Mechanics*, *27*(3), 438–444. https://doi.org/10.1115/1.3644020

Lekka, M., Laidler, P., Gil, D., Lekki, J., Stachura, Z., & Hrynkiewicz, A. Z. (1999). Elasticity of normal and cancerous human bladder cells studied by scanning force microscopy. *European Biophysics Journal*, *28*(4), 312–316. https://doi.org/10.1007/s002490050213

Lim, C. T., Zhou, E. H., & Quek, S. T. (2006). Mechanical models for living cells - a review. *Journal of Biomechanics*, *39*(2), 195–216. https://doi.org/10.1016/j.jbiomech.2004.12.008

Mainardi, F., & Spada, G. (2011). Creep, relaxation and viscosity properties for basic fractional models in rheology. *The European Physical Journal Special Topics*, *193*(1), 133–160. https://doi.org/10.1140/epjst/e2011-01387-1

Moeendarbary, E., & Harris, A. R. (2014). Cell mechanics: Principles, practices, and prospects. *Wiley Interdisciplinary Reviews: Systems Biology and Medicine*, *6*(5), 371–388. https://doi.org/10.1002/wsbm.1275

Moreno-Flores, S., Benitez, R., Vivanco, M. D. M., & Toca-Herrera, J. L. (2010a). Stress relaxation microscopy: Imaging local stress in cells. *Journal of Biomechanics*, *43*(2), 349–354. https://doi.org/10.1016/j.jbiomech.2009.07.037

Moreno-Flores, S., Benitez, R., Vivanco, M. D. M., & Toca-Herrera, J. L. (2010b). Stress relaxation and creep on living cells with the atomic force microscope: A means to calculate elastic moduli and viscosities of cell components. *Nanotechnology*, *21*(44), 445101. https://doi.org/10.1088/0957-4484/21/44/445101

Nawaz, S., Sánchez, P., Bodensiek, K., Li, S., Simons, M., & Schaap, I. A. T. (2012). Cell visco-elasticity measured with AFM and optical trapping at sub-micrometer deformations. *PLoS One*, *7*(9), e45297. https://doi.org/10.1371/journal.pone.0045297

Okajima, T., Tanaka, M., Tsukiyama, S., Kadowaki, T., Yamamoto, S., Shimomura, M., & Tokumoto, H. (2007). Stress relaxation of HepG2 cells measured by atomic force microscopy. *Nanotechnology*, *18*(8), 84010. https://doi.org/10.1088/0957-4484/18/8/084010

Paluch, E. K., Nelson, C. M., Biais, N., Fabry, B., Moeller, J., Pruitt, B. L., Wollnik, C., Kudryasheva, G., Rehfeldt, F., & Federle, W. (2015). Mechanotransduction: Use the force(s). *BMC Biology*, *13*, 47. https://doi.org/10.1186/s12915-015-0150-4

Plodinec, M., Loparic, M., Monnier, C. A., Obermann, E. C., Zanetti-Dallenbach, R., Oertle, P., Hyotyla, J. T., Aebi, U., Bentires-Alj, M., Lim, R. Y., & Schoenenberger, C. A. (2012). The nanomechanical signature of breast cancer. *Nature Nanotechnology*, *7*(11), 757–765. https://doi.org/10.1038/nnano.2012.167

Rotsch, C., & Radmacher, M. (2000). Drug-induced changes of cytoskeletal structure and mechanics in fibroblasts: An atomic force microscopy study. *Biophysical Journal*, *78*(1), 520–535. https://doi.org/10.1016/S0006-3495(00)76614-8

Salbreux, G., Charras, G., & Paluch, E. (2012). Actin cortex mechanics and cellular morphogenesis. *Trends in Cell Biology*, *22*(10), 536–545. https://doi.org/10.1016/j.tcb.2012.07.001

Tavares, S., Vieira, A. F., Taubenberger, A. V., Araújo, M., Martins, N. P., Brás-Pereira, C., Polónia, A., Herbig, M., Barreto, C., Otto, O., Cardoso, J., Pereira-Leal, J. B., Guck, J., Paredes, J., & Janody, F. (2017). Actin stress fiber organization promotes cell stiffening and proliferation of pre-invasive breast cancer cells. *Nature. Communications*, *8*, 1–18. https://doi.org/10.1038/ncomms15237

Weber, A., Iturri, J., Benitez, R., & Toca-Herrera, J. L. (2019). Measuring biomaterials mechanics with atomic force microscopy. 1. Influence of the loading rate and applied force (pyramidal tips). *Microscopy Research and Technique*, *82*, 1392–1400. https://doi.org/10.1002/jemt.23291

Weber, A., Iturri, J., Benitez, R., Zemljic-Jokhadar, S., & Toca-Herrera, J. L. (2019). Microtubule disruption changes endothelial cell mechanics and adhesion. *Scientific Reports*, *9*(1), 1–12. https://doi.org/10.1038/s41598-019-51024-z

Weber, A., Zbiral, B., Iturri, J., Benitez, R., & Toca-Herrera, J. L. (2021). Measuring (biological) materials mechanics with atomic force microscopy. 2. Influence of the loading rate and applied force (colloidal particles). *Microscopy Research and Technique*, *84*(5), 1078–1088. https://doi.org/10.1002/jemt.23643

Wu, P.-H., Aroush, D. R.-B., Asnacios, A., Chen, W.-C., Dokukin, M. E., Doss, B. L., Durand-Smet, P., Ekpenyong, A., Guck, J., Guz, N. V., Janmey, P. A., Lee, J. S. H., Moore, N. M., Ott, A., Poh, Y. C., Ros, R., Sander, M., Sokolov, I., Staunton, J. R., … Wirtz, D. (2018). A comparison of methods to assess cell mechanical properties. *Nature Methods*, *15*(7), 491–498. https://doi.org/10.1038/s41592-018-0015-1

Zemła, J., Danilkiewicz, J., Orzechowska, B., Pabijan, J., Seweryn, S., & Lekka, M. (2017). Atomic force microscopy as a tool for assessing the cellular elasticity and adhesiveness to identify cancer cells and tissues. *Seminars in Cell & Developmental Biology*, *1–10*, 115–124. https://doi.org/10.1016/j.semcdb.2017.06.029

SUPPORTING INFORMATION

Additional supporting information can be found online in the Supporting Information section at the end of this article.

How to cite this article: Weber, A., Benitez, R., & Toca-Herrera, J. L. (2022). Measuring biological materials mechanics with atomic force microscopy - Determination of viscoelastic cell properties from stress relaxation experiments. *Microscopy Research and Technique*, *85*(10), 3284–3295. https://doi.org/10.1002/jemt.24184